Chapter 3

To optimize the processing conditions for development of aerogel using corn starch

3.1 Introduction

Aerogel is a lightweight, porous solid material that is low in density and high in porosity. Polysaccharides, proteins, and other bio-based precursor materials were uncommon in the past for the development of aerogel, but they are now relatively prevalent because of their unique characteristics, such as being less toxic, environmentally friendly, and less dangerous (Nita et al., 2020). Aerogel produced from bio-based precursor materials is utilized for a variety of purposes, including oil-water separation (Meng et al., 2017), thermal insulator (Druel et al., 2017), air filtration (Zeng et al., 2019), ion exchange (Keshipour & Khezerloo, 2017), food packaging (Cristina et al., 2014; de Oliveira, Bruni, el Halal, et al., 2019; de Oliveira, Bruni, Fabra, et al., 2019; Franco et al., 2018; Wang et al., 2018, 2019), food and drug delivery systems (Agostinho et al., 2020; Alnaief et al., 2018; Betz et al., 2012; de Oliveira et al., 2020), etc.

For the production of aerogel, starch is a popular bio-based precursor material. Different kinds of starches were used to create aerogel with a range of functional properties, including those for use as a bioactive filler and carrier in food preparations (Ubeyitogullari & Ciftci, 2016a), a functional food ingredient (Ubeyitogullari et al., 2018), a chemical and bioactive component carrier (Fonseca et al., 2021; García-González, Uy, et al., 2012; Goimil et al., 2017), etc. The two main methods for creating hydrogel are sol-gel (aerogel monoliths) (Franco et al., 2018) and emulsion gelation (aerogel microspheres) (García-González, Uy, et al., 2012). Techniques like supercritical (SC) fluid drying and freeze-drying are frequently employed to convert hydrogel into aerogel. Because supercritical drying preserves the porous structure and creates pores in the nano range, it is superior to freeze drying (Nita et al., 2020).

In recent years, corn starch aerogel has gained interest due to its diverse application potential, especially in the food sector. In earlier research, $SCCO_2$ drying (pressure: 80–200 bar, temperature: 37–45 °C) was used to create aerogel, with a starch concentration ranging from 7–15 % (De Marco & Reverchon, 2017; Druel et al., 2017; Franco et al., 2018; García-González et al., 2015; García-González, Camino-Rey, et al., 2012; García-González, Uy, et al., 2012; García-González & Smirnova, 2013; Goimil et al., 2017; Lovskaya et al., 2015; Mehling et al., 2009; Ubeyitogullari et al., 2018; Zamora-Sequeira et al., 2018; Zheng et al., 2020). A high depressurization rate during $SCCO_2$ drying causes the aerogel's structure to collapse.

Therefore, a slow depressurization rate is usually preferred to minimize the expansion of gas before exiting the aerogel matrix.

Aerogel made of natural polymers has drawbacks such as increased stiffness (which restricts usage in food systems), structural collapse, poor mechanical qualities, etc. (Abdullah et al., 2022). Glycerol is very often used as a plasticizer due to its structural similarity to the glucose unit of starch, more specifically its compatible nature with amylose which enhances its possibility to interact chemically with starch. Glycerol interferes with amylose packing, reducing the intermolecular interactions between the starch molecules. As a result of decreased intramolecular hydrogen bonding along polymer chains, there is an increase in intermolecular space, which increases flexibility and decreases the brittleness of the overall structure (Aghazadeh et al., 2018; Nordin et al., 2020). Glycerol increases the number of hydroxyl groups which increases the affinity of the starch molecules toward water. Moreover, glycerol reduces O-H band stretching which results in strong hydrogen bonds with water (Aghazadeh et al., 2018; Nordin et al., 2020). To the best of our knowledge, there is a lack of study on the effect of glycerol on physical, mechanical, functional, textural, and morphological properties of corn starch aerogel. In the present investigation, we tried to produce corn starch-based aerogel of having good mechanical strength, strong internal structure, and better reusability using glycerol.

3.2 Materials and methods

3.2.1 *Materials*

Native corn starch (amylose content: 13.32%) was purchased from LOBA CHEMIE PVT. LTD. Ethanol (C_2H_5OH: ≥ 99.5% purity) was purchased from Changshu Hongsheng Fine Chemical Co. Ltd. Calcium chloride ($CaCl_2$), potassium chloride (KCl), silica gel, and glycerol were procured from Merck Life Science Private Limited (Mumbai, India).

3.2.2 *Development of cylindrical corn starch aerogel*

The whole preparation process (**Fig. 3.1**) consists of three major steps: (1) hydrogel formation, (2) alcogel formation, and (3) aerogel formation (García-González et al., 2011).

3.2.2.1 *Hydrogel formation*

The hydrogel was prepared as per the method given by Wang et al. (2021). In brief, corn starch (7.5, 10, and 12.5 % w/v) and distilled water were mixed properly, then gelatinized at 93 °C with constant stirring at 450 rpm for 20 min using a laboratory stirrer (PC-420D, CORNING, Mexico). Then, 6 ml of 0.01 % $CaCl_2$ solution and glycerol of varying

concentrations (5, 7.5, and 10 % v/v) were added to the gelatinized starch solution and stirred at 1000 rpm for 10 min. The solution was transferred to a cylindrical polypropylene mold and was kept at 4 °C for 2 days to allow retrogradation. The developed hydrogel was removed from the mold and cut into pieces of 5 mm in length for further studies.

3.2.2.2 *Alcogel formation*

The solvent exchange approach was used to transform the hydrogel into an alcogel (Ubeyitogullari et al., 2018). In brief, the pieces of hydrogel were subjected to four consecutive steps of the solvent (ethanol) transfer process. The pieces were successively submerged in a 10 ml solution of ethanol (30, 50, 70, and 100 %) for 1 h. The pieces were placed into 100 % ethanol for 24 h for the complete removal of water.

3.2.2.3 *Aerogel formation*

Alcogel were dried using supercritical solvents ($SCCO_2$) for 2.5 h at 150 bar pressure, 40 °C temperature with a constant flow rate of 5 g/min. Alcogel was put into the high-pressure chamber of the supercritical drying unit, which was then filled with ethanol (SFE-100-2-C10, WATERS, USA). Due to the constant flow of $SCCO_2$ into the high pressure chamber during the experiment, drying was accomplished. The depressurization was done at a constant temperature for 15 min (Zamora-Sequeira et al., 2018). To ensure the complete removal of ethanol, the amount of ethanol evaporated from the samples was measured at different time intervals by oven drying method (105 °C for 2 h) (Ubeyitogullari & Ciftci, 2016b; Zamora-Sequeira et al., 2018). The dried samples (**Fig. 3.2**) were kept in a desiccator (desiccant: silica gel) for further experiments.

The dimensions (diameter and height) and weight of the hydrogel, alcogel (in all stages of solvent removal), and aerogel were measured using a Vernier caliper (Mitutoyo 532-121, Japan) and electronic balance (ME204, Mettler Toledo, Switzerland), respectively.

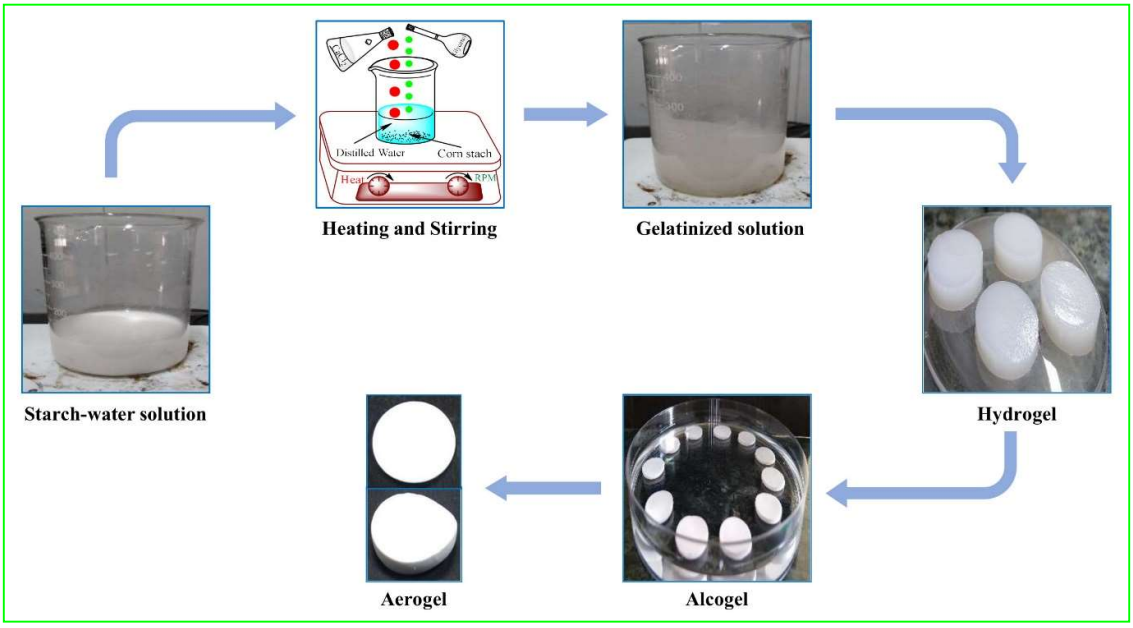

Fig. 3.1 Development of corn starch based aerogel

3.2.3 *Characterization*

3.2.3.1 *Percentage shrinkage, density, and porosity*

3.2.3.1.1 *Percentage shrinkage*

The difference in volume between hydrogel (V_{hyd}) and aerogel (V_{aer}) was used to calculate the total shrinkage percentage (S_T). Moreover, percentage shrinkage during each step (S_1, S_2, S_3, and S_4) of solvent transfer (30, 50, 70, and 100 % ethanol; v/v) and the entire solvent transfer process (S_{ST}: total shrinkage percentage during the entire solvent transfer process) was also calculated from the volume difference observed with respect to V_{hyd}. To calculate V_{hyd}, V_{aer}, the volume of alcogel (V_{alc}), and volume after each step of solvent transfer (V_1 (after 30% ethanol transfer), V_2 (after 50 % ethanol transfer), V_3 (after 70 % ethanol transfer), and V_4 (after 100 % ethanol transfer)), the height and diameter of hydrogel, alcogel, and aerogel were measured. The following formula (**Eq. 3.1**) was used to calculate the total percentage shrinkage (Luo et al., 2019).

$$S_T(\%) = \frac{V_{hyd} - V_{aer}}{V_{hyd}} \times 100 \qquad (3.1)$$

Where, S_T= total shrinkage percentage, V_{hyd}= volume of hydrogel, V_{aer}= volume of aerogel

3.2.3.1.2 *Density and porosity*

Density (ρ) was calculated by dividing mass by volume. The porosity (ε) of the sample is calculated as per **Eq. 3.2** (Ubeyitogullari et al., 2018).

$$\text{Porosity}(\%) = \left(1 - \frac{\rho_b}{\rho_t}\right) \times 100 \quad (3.2)$$

Where, ρ_b=ρ=density of aerogel, ρ_t=ρ_{sk}= skeletal density of corn starch=1.5 g/cm^3

3.2.3.2 *Morphology*

For the morphology study, aerogel pieces (10 mm in diameter and 1 mm thick) were kept under a vacuum. A thin layer of gold was spread over the tops of the samples (de Oliveira, Bruni, el Halal, et al., 2019). Morphology was observed using a scanning electron microscope (JEOL JSM-6390LV, Japan) under an accelerating voltage of 15 kV and at a magnification of 5,500 × and 10,000 ×.

3.2.3.3 *Mechanical performance and recompressibility*

Texture analyzer (TA-XD PLUS, Stable Micro System, UK) with a 30 kg load cell was used to study the mechanical performance. Pre-test and test speed were set at 1 mm/s and 0.1 mm/s respectively, and the compressive strength of aerogel samples was examined under 10, 20, 30, and 50 % strain at room temperature.

For recompressibility, the reciprocating compression of aerogel was performed with 50% compression strain. Meanwhile, the experiment of multiple cycles involving repeated loading-unloading compression (10 times) was carried out for the aerogel.

3.2.3.4 *Crystallinity*

The aerogel samples were exposed to an X-ray beam at 15 mA and 30 kV using an X-ray diffractometer (Miniflex, Rigaku Corporation, Japan). The diffraction angle (2Θ) range was set to 5° to 80° with a step angle of 0.05°. The crystallinity index (CI) or degree of crystallinity was determined through analysis of the diffraction pattern. By joining the lower points of XRD peaks with a smooth line, the amorphous region was separated from the crystalline region. Then the area of the crystalline region was calculated by integrating the area under the peaks. The total area (A_T) (amorphous region and crystalline region) was calculated by integrating the curve over 2Θ between 5° and 80°. Finally, the degree of crystallinity (**Eq. 3.3**) was obtained by dividing the area (A_C) of the crystalline region by the total area (A_T) under the curve (Kumar et al., 2020).

$$\text{Degree of crystallinity}(\%) = \frac{A_C}{A_T} \times 100 \quad (3.3)$$

A_C= area of crystalline region, A_T= total area under the curve

3.2.3.5 ***Thermal behavior***

Thermal properties of the aerogel were determined using a differential scanning calorimeter (DSC 214, NETZSCH, Germany). The sample (5 mg) was loaded into an aluminum pan without the addition of water and was sealed for thermal scanning. Thermal scanning was performed in the temperature range of 25 to 400 °C, under a nitrogen purge (20 ml/min), at a heating rate of 10 °C/min (Franco et al., 2018).

3.2.3.6 ***Hygroscopicity***

The hygroscopicity of aerogel was measured by the method given by Chen and Zhang (2019). About 1 g of aerogel samples were placed on a polypropylene (PP) culture dish and were kept in a desiccator at room temperature at 85% relative humidity. The samples were weighed on a periodical basis at an interval of 24 h till constant weight. The weight gain (%) was calculated using **Eq. 3.4**:

$$\text{Hygroscopicity}\left(\frac{\text{g}}{100\text{g}}\right) = \frac{M_g - M_0}{M_0} \times 100 \quad (3.4)$$

Where, M_0= initial weight of the sample and M_g= gained weight of the sample after every 24 h.

3.2.3.7. ***Water absorption capacity***

The known weight (M_0: approximately 1g) of aerogel samples was placed into 20 ml of distilled water for 30 min. The weight (M_w) of wet samples was taken immediately after wiping out the excess water using filter paper. **Eq. 3.5** was used to calculate the water absorption capacity at 30 min ($WAC_{30\ min}$) (Lin et al., 2012).

$$WAC_{30\ min}(\%) = \frac{M_w - M_0}{M_0} \times 100 \quad (3.5)$$

Where, $WAC_{30\ min}$= water absorption capacity at 30 min, M_W= weight of wet sample after 30 min, M_0= initial weight of the sample

To measure the water absorption capacity at 24 h ($WAC_{24\ h}$), the aerogel samples were kept under the same conditions as discussed in $WAC_{30\ min}$ for 24 h. Aerogel samples were removed

from the water and surface water was wiped off using filter paper. The final weight (M_f) of the samples was taken, and $WAC_{24\ h}$ was calculated by the formula (Equation 6) given by de Oliveira, Bruni, el Halal, et al. (2019).

$$WAC_{24\,h}(\%) = \frac{M_f - M_0}{M_0} \times 100 \quad (3.6)$$

Where, $WAC_{24\ h}$= water absorption capacity at 24 h, M_f= final weight of the sample, M_0= initial weight of the sample

3.2.3.8 *Reusability*

The reusability of aerogel was defined in terms of the repetitive absorbing ability of aerogel after drawing off the water. The samples were first soaked in water for 30 min, and then the weight (M_w) of the wet samples was recorded. Then the soaked samples were dried (hot air oven at 45 °C, overnight) to constant weight and the same procedure was repeated 8 times. Before each stage of soaking the initial weight (M_0) was measured. The values of WAR were calculated using Equation 5 during the whole water absorbing and discharging process (Lin et al., 2012).

3.2.4 *Statistical analysis*

All the analyses were performed in triplicates and the results data were represented as mean ± standard deviation. Statistical analysis was performed using SPSS software (SPSS 17.0, SPSS Inc., Chicago, IL). The data were analyzed by one-way analysis of variance test. The one-way ANOVA was used to compare the means between the samples and determine whether the means of sample is significantly different from each other (Kim, 2017). It serve the purpose of identification whether the addition of glycerol has significant impact or not in the final properties (physico-functional, thermal, mechanical properties etc.) of the samples. Moreover, to know the variation among the samples for a particular quality characteristics of aerogel one way ANOVA was performed. To determine the significant differences among individual results DUNCAN's multiple range test (DMRT) ($p < 0.05$) was performed. In addition to this Duncan Multiple Range Test (DMRT) was performed to know about the nature of variation whether it exhibits significant or non-significant difference between the mean values of samples with respect to all properties. The level of significance was set to $p < 0.05$ to determine the statistical significance. Microsoft Excel 2017 and Origin Pro 2018 (OriginLab, USA) were used for graphing and principal component analysis. The method of PCA consists of several steps. The first step is to collect and arrange the data in a matrix form (rows: samples and

columns: properties). The second step is to subtract the mean of each column from its values to mean centre the data. Then the covariance/correlation matrix is computed and eigenvalue decomposition is performed. Then the eigenvectors are ordered on the basis of decreasing eigenvalues, therefore the first PC explains the most variance. Then the original data is projected onto the principal components (Jolliffe & Cadima, 2016).

3.3 Results and discussion

3.3.1 *Preparation of starch aerogel monoliths*

Native corn starch granules used for the study were in solid form with a smooth and non-porous surface. However, prepared aerogel monoliths were porous in nature even though they were present in solid form. Aerogel preparation involves three sequential phases: hydrogel, alcogel, and aerogel production.

The key variables that affect the gel's texture during hydrogel synthesis are the gelatinization temperature and amylose content (García-González, Uy, et al., 2012; White et al., 2008).In order to promote crystal nucleation with respect to recrystallization and crystal growth and to encourage a more uniform and organized porous network in the resulting aerogel, cross-linker ($CaCl_2$) and glycerol was added to the starch solution after gelatinization at 93 °C. The mixture was then further cooled at 4 °C for 48 h The high critical point of water (Pc = 221 bar; Tc = 374.1 °C) restricts the direct supercritical drying of hydrogel. Additionally, the pressure and temperature required for drying will be higher than the critical conditions that cause starch degradation. To avoid these conditions, solvent exchange was done prior to drying as water is less soluble in $SCCO_2$ hindering the extraction process at supercritical conditions (P_c = 73.8 bar; T_c = 31.1 °C) of CO_2. Therefore, ethanol was selected as the extraction solvent as it is miscible in water and highly soluble in $SCCO_2$.

It is observed (**Fig. 3.2**) that the hydrogel with high starch content (10 and 12.5 %) could not resist the solvent exchange process and a structural breakdown was observed. The higher breakdown was observed for the samples (**Fig. 3.2**) containing higher amount of starch (12.5 %). Therefore, 7.5 % starch content was selected as optimum concentration of starch for the development of aerogel in this study. The resulting starch aerogel monoliths obtained after $SCCO_2$ drying were kept in desiccator for further characterization. The detailed characterization of aerogel monoliths is discussed in the following sections.

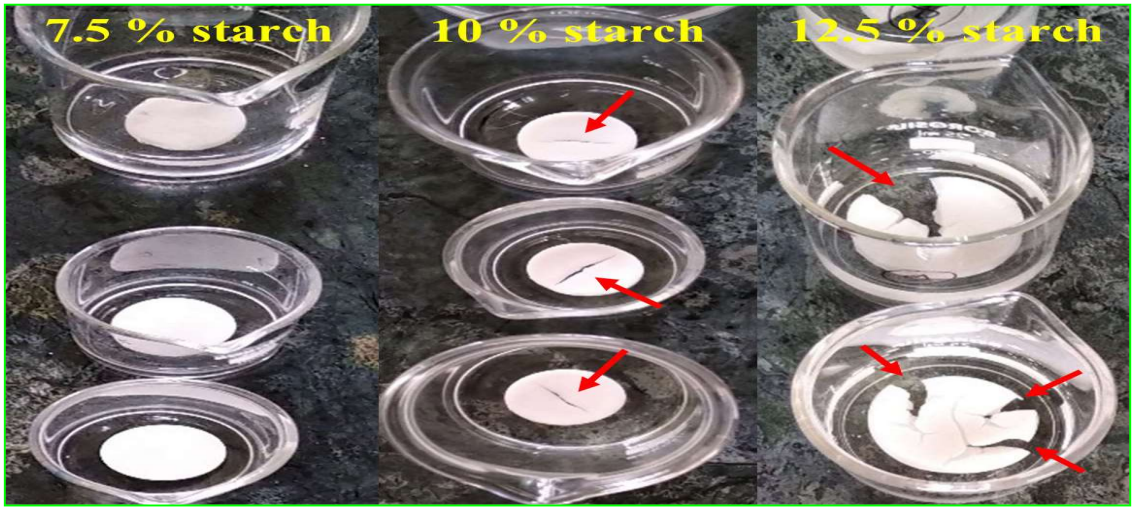

Fig. 3.2 Solvent exchange of hydrogel made of different starch concentrations

3.3.2 *Effect of glycerol on shrinkage and physical characteristics of developed aerogel*

The shrinkage characteristics [shrinkage (%) during each stage of solvent transfer, S_{ST} (total shrinkage percentage during the entire solvent transfer process), and S_T (total shrinkage percentage)] of native corn starch and glycerol-added aerogel are presented in **Fig. 3.3**. Throughout the 48 h of aging of all the hydrogel samples, no discernible shrinkage was found. However, during each stage of the solvent transfer process volume shrinkage was observed (**Fig. 3.3a**). Significant difference ($p < 0.05$) in S_T values was observed in glycerol-added samples in comparison to the control samples (**Fig. 3.3b**). Lesser shrinkage was observed during drying as compared to S_{ST}. The higher shrinkage during solvent transfer may be attributed to the reduced surface tension (decrease in capillary force) with the increasing concentration of ethanol. The reduction in capillary force leads to reverse the flow direction from gel matrix to bulk solution and so gel volume decreases (Mehling et al., 2009). The glycerol-added aerogel showed higher percentage shrinkage as compared to the control samples (75.03 %) and the S_T values of aerogel were increased with the increase in glycerol concentration from 5-10 %. Shrinkage during supercritical drying of samples leads to changes in S_T values. Moreover, a significant difference was observed between the control sample (75.03 %) and the 10% glycerol-added sample (78.00 %). Aerogel with more glycerol may shrink more because the surface tension inside the aerogel matrix decreases (García-González, Uy, et al., 2012).

The density of glycerol-added aerogel differ significantly from the control sample however, lower concentrations of glycerol showed an insignificant impact on the density of aerogel. The density of aerogel increased gradually with the increase in the concentration of glycerol from

5 to 10 % (**Fig 3.4**). The porosity of the sample decreased when glycerol concentration increased from 0 to 7.5 % however, beyond that point, no discernible effect could be seen (**Fig. 3.4**). The decrease in porosity is associated with an increase in density. The increase in density and reduction in the porosity of glycerol-added samples may be attributed to the development of a thick and more connected network (due to the formation of hydrogen bonds between polymer chains upon efficient action of glycerol) within the internal matrix of aerogel (de Oliveira et al., 2021; Fontes-Candia et al., 2019; Ubeyitogullari et al., 2018). Aerogel's higher density may also be influenced by the increased shrinkage percentage, which makes the structure more compact. The specific surface area of the aerogel samples was in the range of 7.91 to 13.26 m^2/g.

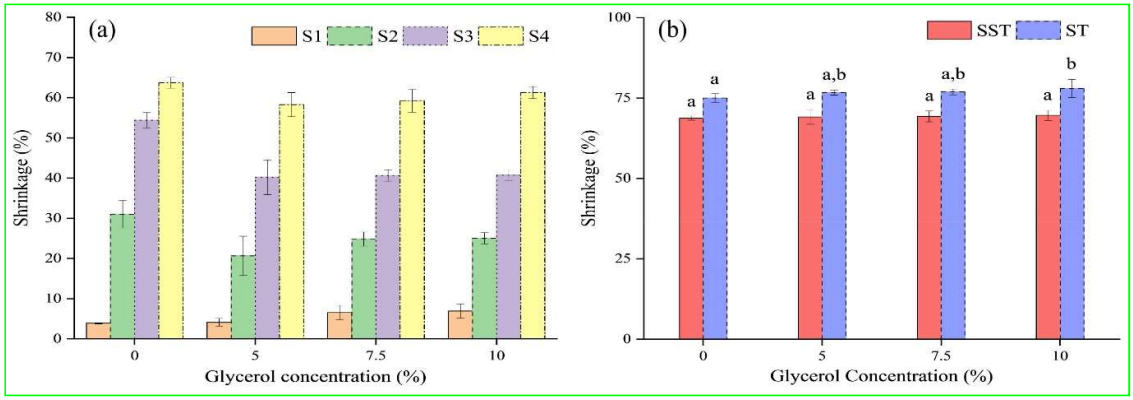

Fig. 3.3 Shrinkage during each stage of solvent transfer (a) and total shrinkage after solvent transfer and drying (b)

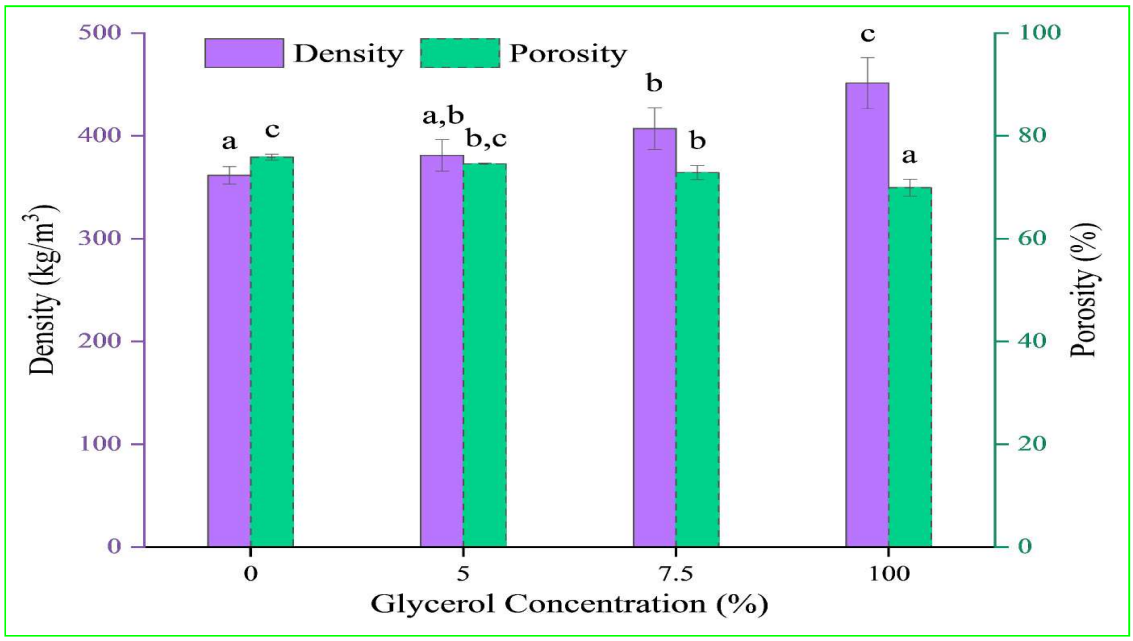

Fig. 3.4 Density and porosity of the developed aerogel

3.3.3 *Effect of glycerol on morphology of developed aerogel*

The pores of the developed aerogel were up to 400 nm in size (**Fig. 3.5**). Macrospores and an open network of the control sample (**Fig. 3.5b**) may be attributed to the bursting of swollen starch granules (Glenn et al., 2008). The addition of glycerol increased the interconnections inside the matrix and favors the thick fibrils development which produced a dense and homogeneous structure (**Fig. 3.5d** and **Fig. 3.5f**) (Ubeyitogullari et al., 2018). Development of thick fibrils inside the aerogel matrix was observed to be increased with the increase in glycerol concentration (**Fig. 3.5c** to **Fig. 3.5f**). Thinner fibrils constituted network was observed in the control sample which was supported by the findings of Ubeyitogullari et al. (2018).

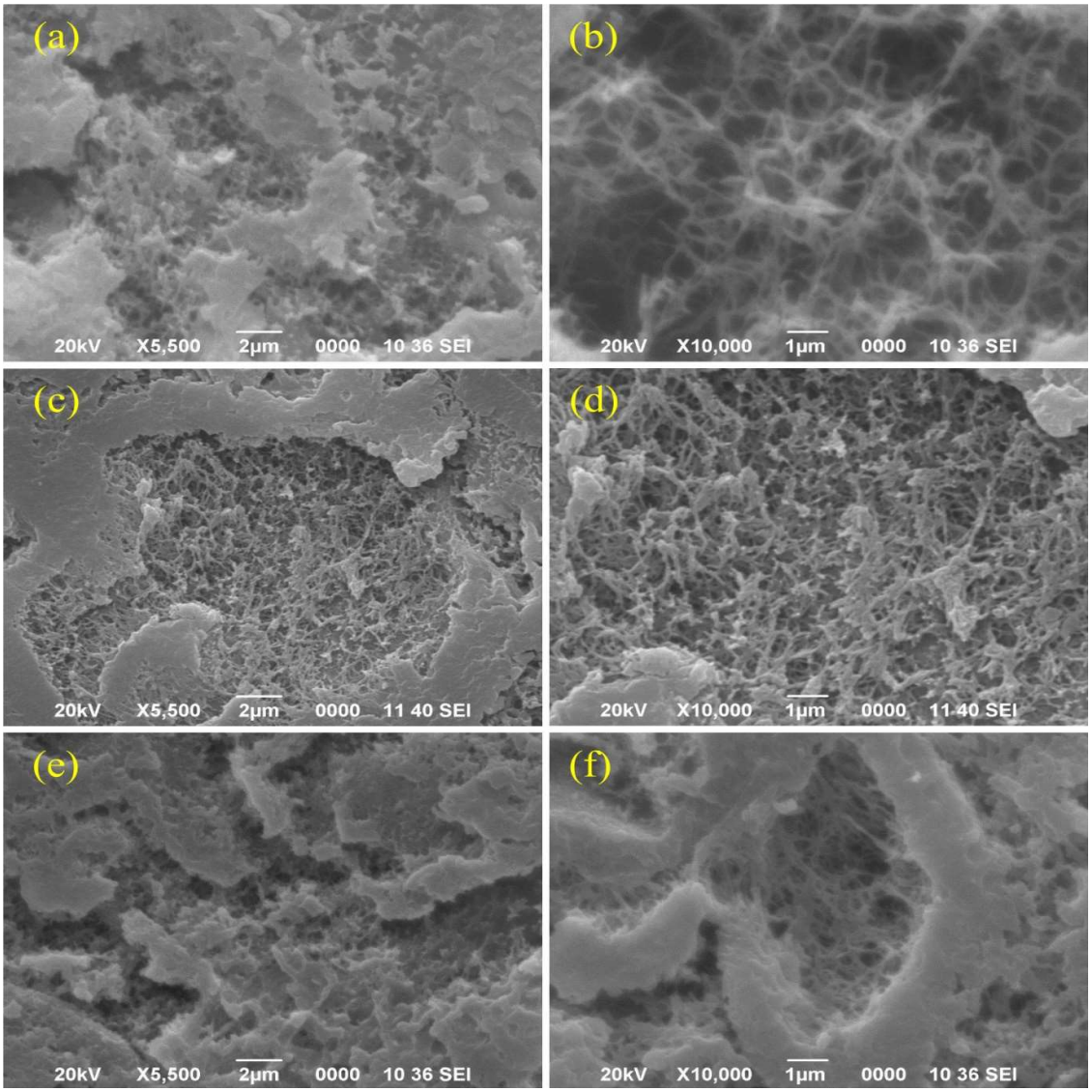

Fig. 3.5 SEM images of control (a, & b), 5 % glycerol added (c & d) and 10 % glycerol added (e, & f) aerogel

3.3.4 *Effect of glycerol on mechanical properties of aerogel*

The repetitive compression test defines the ability of aerogel to retain its texture and integrity under successive loading-unloading. Glycerol-added aerogel retained their structure even after 10 cycles of successive compression. This may be due to the presence of many interconnections in glycerol-based aerogels (**Fig. 3.6**). An increase in compressive force was observed during the initial stages of successive compression, and after a few cycles, the compressive force became approximately constant (**Fig. 3.6**) in all the aerogel samples except the control. The increase in compressive force may be attributed to the development of a more compact structure after compression however, a constant compressive force may be attributed to the development of maximum possible interconnections during compression. After all compression cycles, the total changes in compressive force were quite high (28.00–344.43 N) in the control aerogel, but they were only 18.53–22.74% in the glycerol-based aerogel. The higher changes may be related to the development of interconnected and more compact structures from the existing porous and loose structures due to physical cross-linking upon compression. However, glycerol-based aerogel possesses only minor changes in compressive force which confirms its structure maintaining capability.

Compressive strength at different strain values was estimated to understand the mechanical behavior of both the control and glycerol-added aerogel (**Fig. 3.7**). Compressive strength value is increased progressively along with the increasing strain values in all the samples. This may be attributed to a more compact structure resulting in a higher strain. The addition of glycerol significantly changed ($p < 0.05$) the compressive strength values of aerogel, however in the lower strain (10 and 20 %) values, the difference in compressive strength is not significant among the samples as compared to the values obtained in higher strain (30 and 50%). The mechanical toughness of aerogel depends mainly on the bulk density and pore size (Takeshita & Yoda, 2017). Glycerol contributed to higher compressive strength, so glycerol-added samples had higher compressive strength than the control sample. This may be due to the dense structure of the glycerol-added aerogel. The density and porosity values of glycerol-added aerogel is supporting the compressive strength values. The decrease in the density of aerogels might be related to a decrease in the stiffness of the aerogel network (Xiao et al., 2018; Zhu et al., 2019). The present study may be helpful in finding the application of corn starch-based aerogel as a structural material in transportation, kinetic energy absorber material, cushioning material, etc.

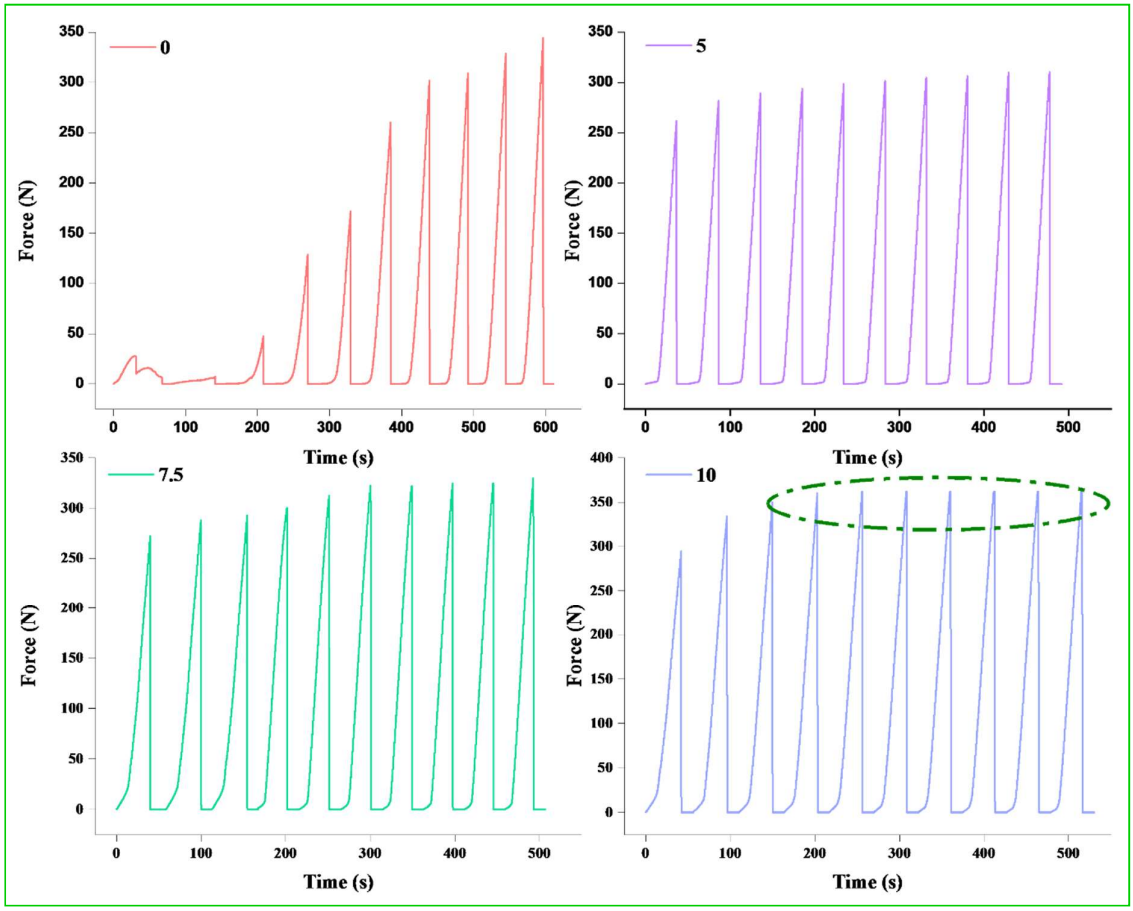

Fig. 3.6 Recompressibility of control (0) and 5, 7.5, and 10 % glycerol added aerogel

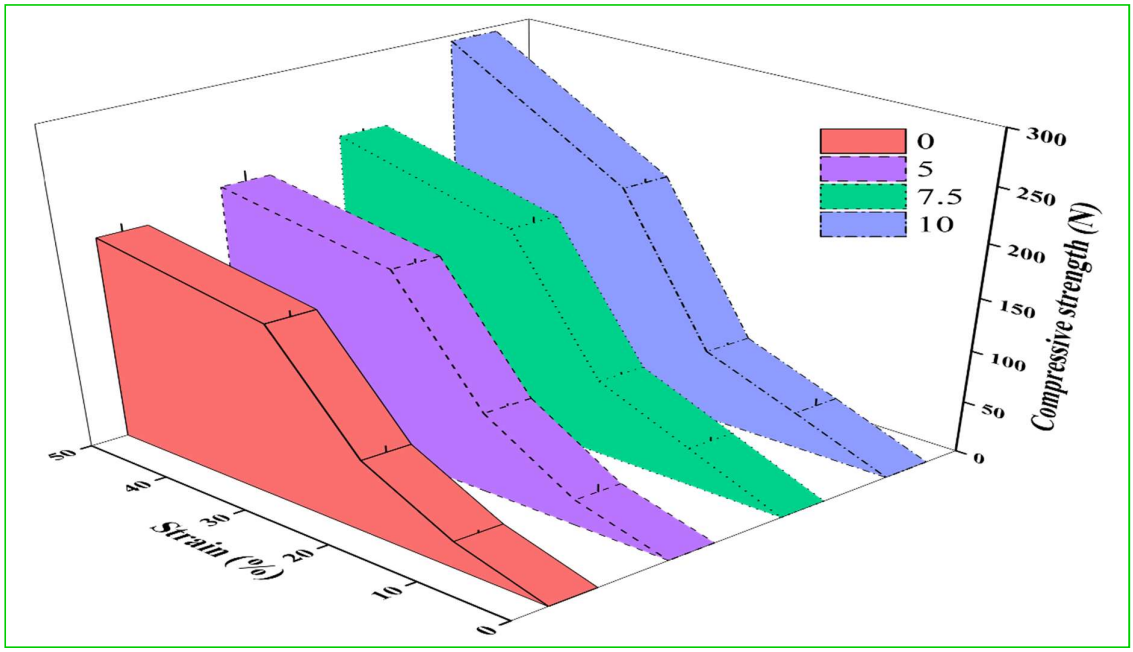

Fig. 3.7 Recompressibility of control (0) and 5, 7.5, and 10 % glycerol added aerogel

3.3.5 *Effect of glycerol on crystalline behavior of aerogel*

The retrogradation of thermoplastic starch was studied through the XRD technique, which is usually used to assess the difference in hydrogen bond formation between starch aerogel. The retrogradation of starch plays an important role in association with starch crystallinity (Aghazadeh et al., 2018). The XRD patterns representing the crystallinity of the aerogel were shown in **Fig. 3.8**. At about 2Θ = 17, 19, 21, and 23°, major diffraction peaks were observed in all aerogel along with one minor peak at about 2Θ = 34°, which suggests the formation of B-type polymorph as well as the formation of amylose-lipid inclusion complexes that represents a crystalline structure (Enrione et al., 2007; Zhu, 2019). The crystallinity index (CI) ranges from 20.75 to 37.87 % (**Fig. 3.8**). The pure corn starch aerogel had the lowest CI (20.75 %) however, the CI value increases with the increased concentration of glycerol in aerogel. Glycerol increases the free volume in the starch polymer matrix, which can promote starch chain mobility and encourage crystallite development (Aghazadeh et al., 2018). The addition of glycerol may increase the alignment of polymer crystals and form a more regular and crystalline area with sharp peaks. Moreover, the formation of an interconnected network may lead to an increase in the CI value (Abhari et al., 2017). Abhari et al. (2017) reported a similar increment in CI values of citric acid-cross-linked gel samples. The antiplasticization effect of glycerol might be the reason for greater rigidity in glycerol-added aerogel. Strong interactions between glycerol and polymers cause a reorganization of the polymer network, which helps crystallization and makes the chain stiffer (Genkina et al., 2014).

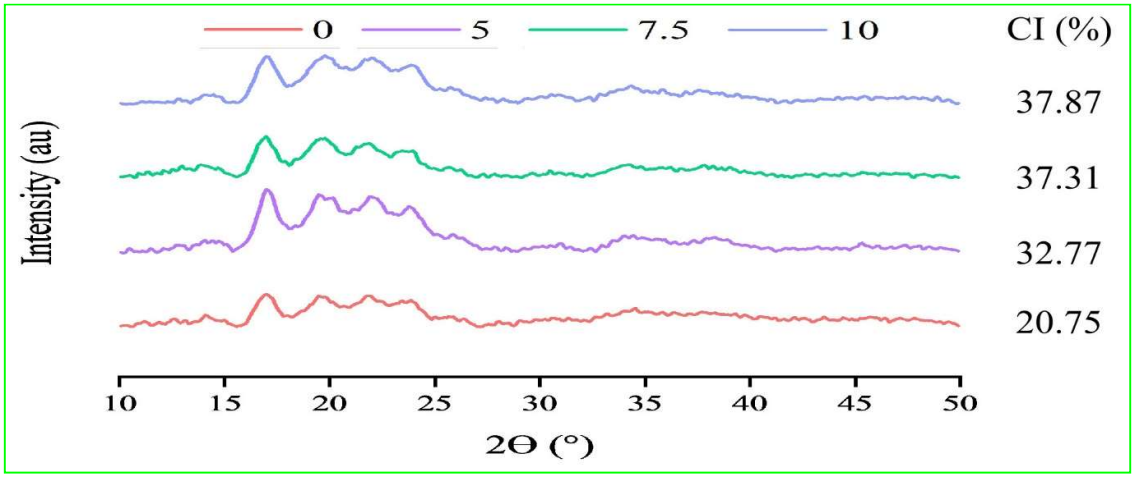

Fig. 3.8 X-ray diffraction pattern and crystallinity index (CI) of control (0) and 5, 7.5, and 10 % glycerol added aerogel

3.3.6 *Effect of glycerol on thermal properties of aerogel*

The thermal behavior of aerogel was explained by the data obtained and represented in the DSC (**Table 3.1**). The characteristic endothermic peaks (due to dehydration and gelatinization of aerogel) are termed as gelatinization temperature. Melting of amylopectin crystalline lamellae and/or disruption of double helices formed by H-bonds within amylopectin side chains leads to develop these endothermic regions (Genkina et al., 2014). The enthalpy of gelatinization was observed to be decreased as the glycerol concentration increased (382 < 325.6 < 265.1 J/g). The gelatinization enthalpy of the control aerogel was 341.7 J/g. The higher gelatinization enthalpy in glycerol-added aerogel may be attributed to the interaction of glycerol within starch molecules which formed more thermally stable aerogel (Chen & Zhang, 2019). Moreover, onset temperature (T_o) and end temperature (T_e) were observed to be decreased followed by an increase with the increase of glycerol concentration (Table 3.1). Aerogels with 5% glycerol added had significantly higher onset, end, and peak temperature (T_p) values than control aerogel (**Table 3.1**). The preferential destruction of starch granules may be due to the rise in onset temperature however, the rise in peak temperature may be caused by the rearrangement of deformed starch chains, interaction with adjacent chains, and/or attainment of crystalline stability (Kumar et al., 2020). These characteristics may enable the use of aerogel as heat storage sorbents (Pierre & Pajonk, 2002).

Table 3.1 Thermal properties of aerogel

Glycerol concentration (%)	Onset temperature (° C)	Peak temperature (° C)	End Temperature (° C)
0	48.6	84.4	134.4
5	56.4	98.4	145.0
7.5	42.3	81.6	130.9
10	47.5	85.9	128.9

3.3.7 *Effect of glycerol on hygroscopicity of aerogel*

The hygroscopic behavior of the aerogel was observed for 10 consecutive days and the moisture taking capacity (cumulative basis) of the aerogel was represented in **Fig. 3.9**. The water gain from the humid environment is dependent on the porous structure and composition of the aerogel (Arboleda et al., 2013). On day 1, the percentage of weight gain was the highest, and the cumulative weight gain increased gradually after that (**Fig. 3.9**). Aerogel with 10 % glycerol had 9.16 % equilibrium moisture content, which was much higher than the control (8.74 %) and aerogel with 5 % glycerol level. The water uptake phenomenon may be attributed

to the inherent affinity of both starch and glycerol toward the water (Arboleda et al., 2013; Chen & Zhang, 2019). The moisture migration through the aerogel is facilitated due to an increase in free volume as discussed in section 3.3.5. Moreover, glycerol forms cluster with itself at its high concentration which increases inter-chain spacing (due to the inclusion of glycerol) between polymer chains that may promote the diffusion of water vapor into the aerogel matrix (Ollé Resa et al., 2014). The limited changes in equilibrium moisture may be amalgamated into the porous or capillary structure of aerogel (Chen & Zhang, 2019).

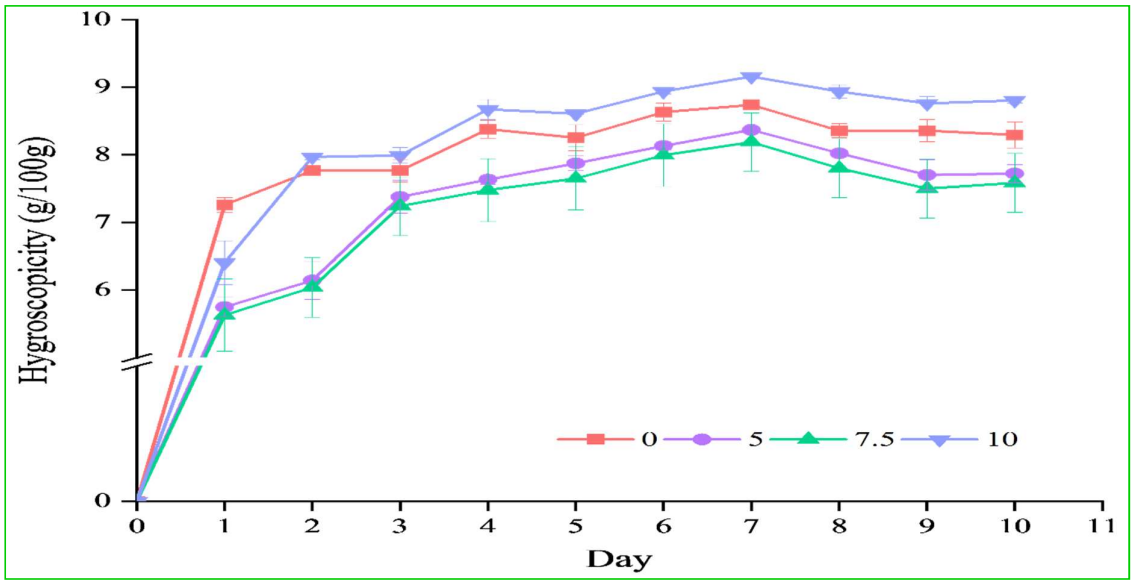

Fig. 3.9 Hygroscopicity of control (0) and 5, 7.5, and 10 % glycerol added aerogel

3.3.8 *Effect of glycerol on water absorption capacity (WAC) of aerogel*

The level of glycerol had an insignificant effect on the $WAC_{30\ min}$ value of aerogel however, glycerol-based aerogel had significantly different $WAC_{30\ min}$ values than control aerogel (**Fig. 3.10**). Among all aerogel, control aerogel has the highest $WAC_{30\ min}$. The lower value of $WAC_{30\ min}$ in glycerol-added aerogel may be due to their dense structure which does not permit rapid water intake through the capillary structure. However, the less compact structure of control aerogel permits rapid water uptake through its capillary structure.

The amount of empty spaces (porosity) in the 3D (three-dimensional) network of aerogel regulates the water absorption process, density is another important factor that has a direct influence on absorption and its entrapping capacity (Fonseca et al., 2021). Control aerogel and 7.5 % glycerol-added aerogel showed nearly similar $WAC_{24\ h}$ values (**Fig. 3.10**). The impact of glycerol on the $WAC_{24\ h}$ of glycerol-added aerogel was insignificant at higher concentrations however, 5 % glycerol containing aerogel had significantly different $WAC_{24\ h}$ (211.85%) which

may be due to the combined effect of porosity or capillary structure and affinity of glycerol. The addition of glycerol may have increased the number of hydroxyl groups in the aerogel matrix. As a result, the aerogel's ability to hold water may have also increased (Nordin et al., 2020). But an aerogel with a higher percentage of glycerol has a lower $WAC_{24\ h}$ because its structure is dense and has fewer pores.

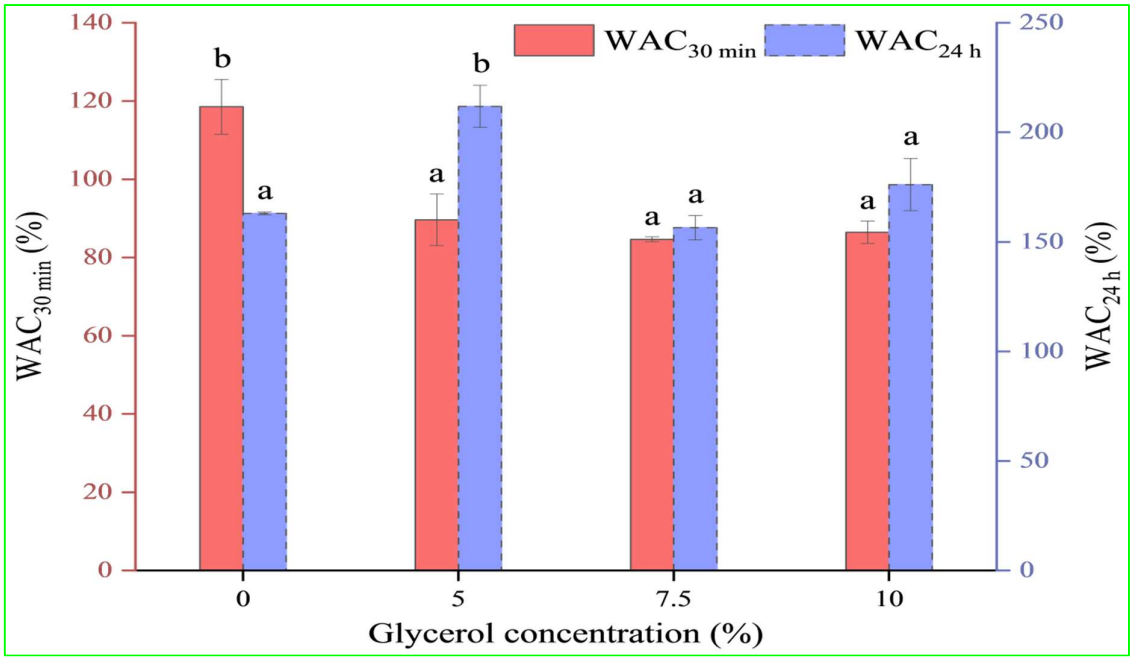

Fig. 3.10 Water absorption capacity at 30 min ($WAC_{30\ min}$) and 24 h ($WAC_{24\ h}$) of aerogel

3.3.9. *Effect of glycerol on reusability of aerogel*

Reusability is the performance measurement of the structural stability of the aerogel. The reusability was measured by the repetitive water absorbing-discharging process of aerogel which ultimately determines its structural stability. The control aerogel can only resist up to four times repetitive water absorbing-discharging process and then started to disintegrate (**Fig. 3.11**). Similar observation was documented by Wu et al. (2019) in pure cellulose nanofibril aerogel. But adding glycerol makes the structure dense and uniform, so the aerogel that contains glycerol can withstand even after eight cycles of water absorbing and discharging process. (**Fig. 3.11**). Water absorption value of all the samples is decreased with the repetitive water absorbing-discharging process. Nevertheless, it was also observed that in the case of control aerogel, the water absorption value is increased, and it may be due to the collapse of the internal matrix. A similar kind of increased water absorption was observed in aerogel having the lowest concentration of glycerol after experiencing six repetitive water absorbing-discharging processes.

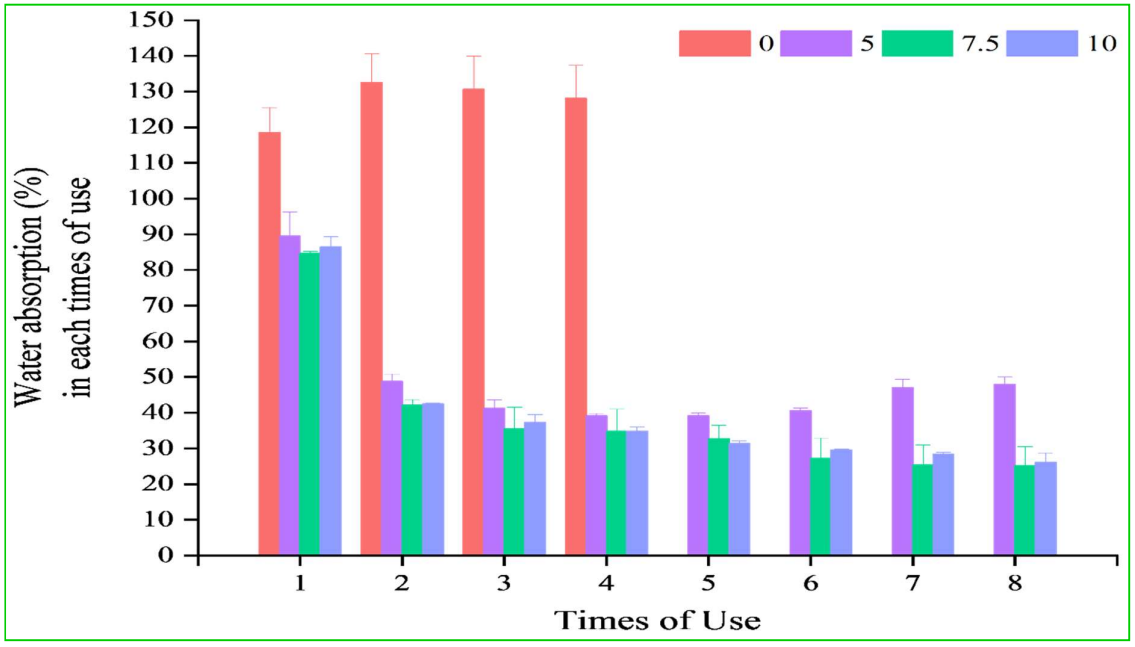

Fig. 3.11 Reusability of control (0) and 5, 7.5, and 10 % glycerol added aerogel

3.3.10 *Principal component analysis (PCA)*

To visualize the effect of glycerol concentration on the physico-functional, thermal, and mechanical properties of corn starch aerogel PCA biplot was used. More specifically, in present study PCA was used to show the correlation between the properties represented by the term loading plot whether they exhibited a positive correlation or a negative correlation with the other or with a cluster of properties existing near a score. The scores present on the figures depicted the samples having different concentration of glycerol. Moreover, this study present the properties (loading plot) nearly associated with a sample (score). How the effect of glycerol regulated the properties (physico-functional, thermal, and mechanical properties) of aerogel and the respective trends corresponds to the each sample was in line with the position of scores and loading plot in the PCA biplot. The PCA was performed without any pre-processing of data using 4 number of samples (C0- control sample (0 % glycerol), G5, G7.5, and G10 are samples containing 5, 7.5, and 10 % glycerol respectively) and 18 numbers of variables (S1, S2, S3, and S4 are % shrinkage during 30, 50, 70, and 100 % ethanol transfer with respect to hydrogel volume, SST-% shrinkage during total ethanol transfer process, ST- total % shrinkage, ρ- density, ε- porosity, WAC- water absorption capacity, WAR- water absorption rate, CI- crystallinity index (%), CS10, CS20, CS30, and CS50 are compressive strength against 10, 20, 30, and 50 % strain respectively, To, Tp, and Te are onset, peak, and end temperature respectively.) which was represented in the biplot as scores and loading plot

respectively. The algorithm used in present study was Eigen-decomposition of the covariance/correlation matrix. The biplot (**Fig. 3.12**) represents 92.05 % of variations, which is the simple way to correlate scores (glycerol concentration) with loadings (properties). A positive correlation is exhibited by a unidirectional loading plot, whereas a negative correlation is expressed by the loading plots generated in the opposite direction. Moreover, no correlation is exhibited by the orthogonal plots. It was observed that maximum properties are highly associated with glycerol-added samples. However, the cluster corresponding to G5 showed a negative correlation on properties like $WAC_{24\ h}$, CS 20 (compressive strength at 20 % strain), T_p, T_e, and T_o with respect to the cluster corresponding to G7.5 and G10 [representing properties like S1 (shrinkage during 30% ethanol substitution in hydrogel), CS 10 (compressive strength at 10 % strain), CS 50 (compressive strength at 50 % strain), and ρ]. Moreover, other properties like CI, SST (total percentage shrinkage of hydrogel during the entire solvent transfer process), ST (total shrinkage of hydrogel during the entire aerogel making process), CS 30 (compressive strength at 30 % strain) are unidirectional to properties corresponds to clusters of G7.5 and G10. This may be due to higher concentrations of glycerol having a significant effect on these properties. Nevertheless, it was observed that another cluster formed corresponding to C0 showed a positive correlation to G5 and a negative correlation to G7.5 and G10. PCA plot provided important insight into how all the properties are related to each other with different glycerol concentrations.

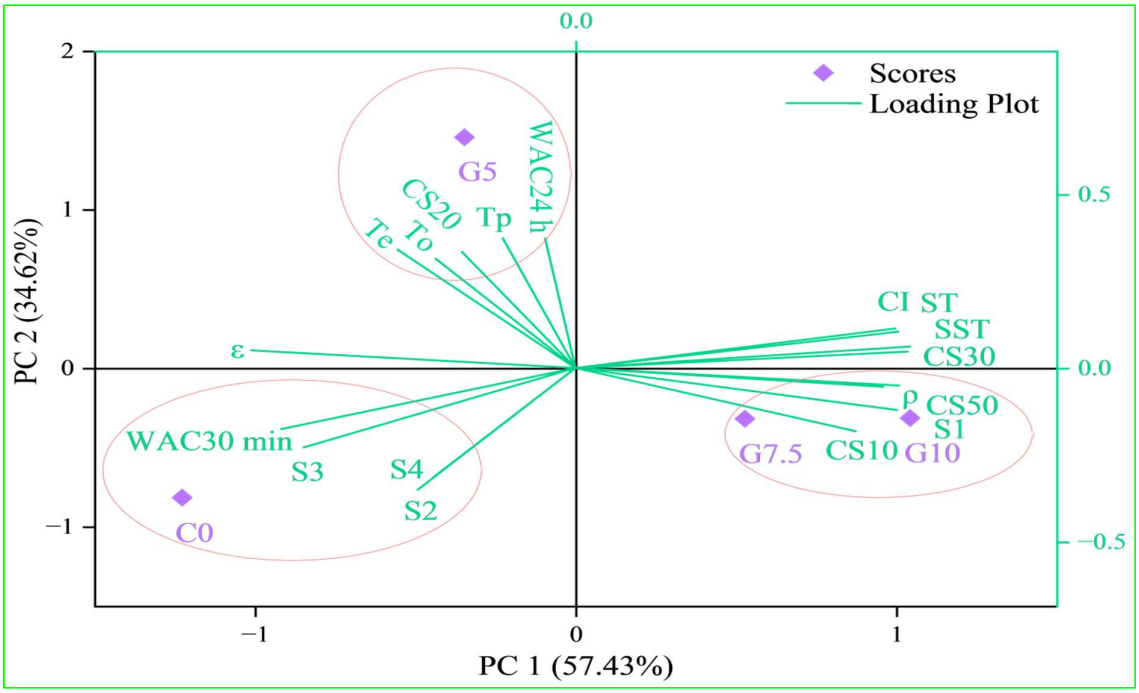

Fig. 3.12 Principal component analysis (PCA) plot of characteristics of aerogel

3.4 Conclusion

This study demonstrates the effect of different concentrations of glycerol on physico-functional, morphological, rehydration, mechanical, and thermal properties of corn starch aerogel and emphasizes the application of thin aerogel monoliths. The addition of glycerol significantly improved the internal matrix, $WAC_{24\ h}$, CI, hygroscopicity, reusability, and mechanical properties. Among three different concentrations of glycerol, the higher two concentrations showed a similar impact on the aforesaid properties. However, in terms of porous nature, glycerol-based aerogel showed less porosity and a denser structure. It was found that the samples containing no glycerol are more porous and less dense which is crucial in aerogel however hygroscopicity, reusability, and mechanical properties are also important and were found better in glycerol-added aerogel. These properties will help to find a broad area of its potential application like sensing, moisture absorber, repeated use in water, smart packaging, etc. Physico-mechanical properties of corn starch-based aerogel was successfully improved using glycerol.

3.5 References

Abdullah, Zou, Y. C., Farooq, S., Walayat, N., Zhang, H., Faieta, M., Pittia, P., & Huang, Q. (2022). Bio-aerogels: Fabrication, properties and food applications. *Critical Reviews in Food Science and Nutrition*, *63*(24), 6687-6709.

Abhari, N., Madadlou, A., & Dini, A. (2017). Structure of starch aerogel as affected by crosslinking and feasibility assessment of the aerogel for an anti-fungal volatile release. *Food Chemistry*, *221*, 147–152.

Aghazadeh, M., Karim, R., Rahman, R. A., Sultan, M. T., Johnson, S. K., & Paykary, M. (2018). Effect of glycerol on the physicochemical propertiesof cereal starch films. *Czech Journal of Food Sciences*, *36*(5), 403–409.

Agostinho, D. A. S., Paninho, A. I., Cordeiro, T., Nunes, A. V. M., Fonseca, I. M., Pereira, C., Matias, A., & Ventura, M. G. (2020). Properties of κ-carrageenan aerogels prepared by using different dissolution media and its application as drug delivery systems. *Materials Chemistry and Physics*, *253*, 123290.

Alnaief, M., Obaidat, R., & Mashaqbeh, H. (2018). Effect of processing parameters on preparation of carrageenan aerogel microparticles. *Carbohydrate polymers*, *180*, 264-275.

Arboleda, J. C., Hughes, M., Lucia, L. A., Laine, J., Ekman, K., & Rojas, O. J. (2013). Soy

protein-nanocellulose composite aerogels. *Cellulose*, *20*(5), 2417–2426.

Betz, M., García-González, C. A., Subrahmanyam, R. P., Smirnova, I., & Kulozik, U. (2012). Preparation of novel whey protein-based aerogels as drug carriers for life science applications. *Journal of Supercritical Fluids*, *72*, 111–119.

Chen, K., & Zhang, H. (2019). Alginate/pectin aerogel microspheres for controlled release of proanthocyanidins. *International Journal of Biological Macromolecules*, *136*, 936–943.

Cristina, A., Souza, D., Dias, A. M. A., Sousa, H. C., & Tadini, C. C. (2014). Impregnation of cinnamaldehyde into cassava starch biocomposite films using supercritical fluid technology for the development of food active packaging. *Carbohydrate Polymers*, *102*, 830–837.

De Marco, I., & Reverchon, E. (2017). Starch aerogel loaded with poorly water-soluble vitamins through supercritical CO2 adsorption. *Chemical Engineering Research and Design*, *119*, 221–230.

de Oliveira, A. C. S., Ugucioni, J. C., & Borges, S. V. (2021). Effect of glutaraldehyde/glycerol ratios on the properties of chitosan films. *Journal of Food Processing and Preservation*, *45*(1), 0–3.

de Oliveira, J. P., Bruni, G. P., el Halal, S. L. M., Bertoldi, F. C., Dias, A. R. G., & Zavareze, E. da R. (2019). Cellulose nanocrystals from rice and oat husks and their application in aerogels for food packaging. *International Journal of Biological Macromolecules*, *124*, 175–184.

de Oliveira, J. P., Bruni, G. P., Fabra, M. J., da Rosa Zavareze, E., López-Rubio, A., & Martínez-Sanz, M. (2019). Development of food packaging bioactive aerogels through the valorization of Gelidium sesquipedale seaweed. *Food Hydrocolloids*, *89*, 337–350.

de Oliveira, J. P., Bruni, G. P., Fonseca, L. M., da Silva, F. T., da Rocha, J. C., & da Rosa Zavareze, E. (2020). Characterization of aerogels as bioactive delivery vehicles produced through the valorization of yerba-mate (Illex paraguariensis). *Food Hydrocolloids*, *107*, 105931.

Druel, L., Bardl, R., Vorwerg, W., & Budtova, T. (2017). Starch Aerogels: A Member of the Family of Thermal Superinsulating Materials. *Biomacromolecules*, *18*(12), 4232–4239.

Enrione, J. I., Hill, S. E., & Mitchell, J. R. (2007). Sorption behavior of mixtures of glycerol and starch. *Journal of Agricultural and Food Chemistry*, *55*(8), 2956–2963.

Fonseca, L. M., Silva, F. T. da, Bruni, G. P., Borges, C. D., Zavareze, E. da R., & Dias, A. R. G. (2021). Aerogels based on corn starch as carriers for pinhão coat extract (Araucaria angustifolia) rich in phenolic compounds for active packaging. *International Journal of Biological Macromolecules*, *169*, 362–370.

Fontes-Candia, C., Erboz, E., Martínez-Abad, A., López-Rubio, A., & Martínez-Sanz, M. (2019). Superabsorbent food packaging bioactive cellulose-based aerogels from Arundo donax waste biomass. *Food Hydrocolloids*, *96*, 151–160.

Franco, P., Aliakbarian, B., Perego, P., Reverchon, E., & De Marco, I. (2018). Supercritical Adsorption of Quercetin on Aerogels for Active Packaging Applications. *Industrial and Engineering Chemistry Research*, *57*(44), 15105–15113.

García-González, C. A., Alnaief, M., & Smirnova, I. (2011). Polysaccharide-based aerogels—Promising biodegradable carriers for drug delivery systems. *Carbohydrate polymers*, *86*(4), 1425-1438.

García-González, C. A., Camino-Rey, M. C., Alnaief, M., Zetzl, C., & Smirnova, I. (2012). Supercritical drying of aerogels using CO 2: Effect of extraction time on the end material textural properties. *Journal of Supercritical Fluids*, *66*, 297–306.

García-González, C. A., Jin, M., Gerth, J., Alvarez-Lorenzo, C., & Smirnova, I. (2015). Polysaccharide-based aerogel microspheres for oral drug delivery. *Carbohydrate Polymers*, *117*, 797–806.

García-González, C. A., & Smirnova, I. (2013). Use of supercritical fluid technology for the production of tailor-made aerogel particles for delivery systems. *Journal of Supercritical Fluids*, *79*, 152–158.

García-González, C. A., Uy, J. J., Alnaief, M., & Smirnova, I. (2012). Preparation of tailor-made starch-based aerogel microspheres by the emulsion-gelation method. *Carbohydrate Polymers*, *88*(4), 1378–1386.

Genkina, N. K., Kozlov, S. S., Martirosyan, V. V., & Kiseleva, V. I. (2014). Thermal behavior of maize starches with different amylose/amylopectin ratio studied by DSC analysis. *Starch/Staerke*, *66*(7–8), 700–706.

Glenn, G. M., Klamczynski, A., Chiou, B. Sen, Orts, W. J., Imam, S. H., & Wood, D. F. (2008). Temperature related structural changes in wheat and corn starch granules and their effects

on gels and dry foam. *Starch/Staerke*, *60*(9), 476–484.

Goimil, L., Braga, M. E. M., Dias, A. M. A., Gómez-Amoza, J. L., Concheiro, A., Alvarez-Lorenzo, C., De Sousa, H. C., & García-González, C. A. (2017). Supercritical processing of starch aerogels and aerogel-loaded poly(ε-caprolactone) scaffolds for sustained release of ketoprofen for bone regeneration. *Journal of CO2 Utilization*, *18*, 237–249.

Jolliffe, I. T., & Cadima, J. (2016). Principal component analysis: a review and recent developments. *Philosophical transactions of the royal society A: Mathematical, Physical and Engineering Sciences*, *374*(2065), 20150202.

Keshipour, S., & Khezerloo, M. (2017). Gold nanoparticles supported on cellulose aerogel as a new efficient catalyst for epoxidation of styrene. *Journal of the Iranian Chemical Society*, *14*(5), 1107–1112.

Kim, T. K. (2017). Understanding one-way ANOVA using conceptual figures. *Korean journal of anesthesiology*, *70*(1), 22.

Kumar, Y., Singh, L., Sharanagat, V. S., Patel, A., & Kumar, K. (2020). Effect of microwave treatment (low power and varying time) on potato starch: Microstructure, thermo-functional, pasting and rheological properties. *International Journal of Biological Macromolecules*, *155*, 27–35.

Lin, N., Bruzzese, C., & Dufresne, A. (2012). TEMPO-oxidized nanocellulose participating as crosslinking aid for alginate-based sponges. *ACS Applied Materials and Interfaces*, *4*(9), 4948–4959.

Lovskaya, D. D., Lebedev, A. E., & Menshutina, N. V. (2015). Aerogels as drug delivery systems: In vitro and in vivo evaluations. *Journal of Supercritical Fluids*, *106*, 115–121.

Luo, Q., Huang, X., Gao, F., Li, D., & Wu, M. (2019). Preparation and characterization of high amylose corn starch-microcrystalline cellulose aerogel with high absorption. *Materials*, *12*(9), 1420.

Mehling, T., Smirnova, I., Guenther, U., & Neubert, R. H. H. (2009). Polysaccharide-based aerogels as drug carriers. *Journal of Non-Crystalline Solids*, *355*(50–51), 2472–2479.

Meng, G., Peng, H., Wu, J., Wang, Y., Wang, H., Liu, Z., & Guo, X. (2017). Fabrication of superhydrophobic cellulose/chitosan composite aerogel for oil/water separation. *Fibers and Polymers*, *18*(4), 706-712.

Nita, L. E., Ghilan, A., Rusu, A. G., Neamtu, I., & Chiriac, A. P. (2020). New trends in bio-based aerogels. *Pharmaceutics*, *12*(5).

Nordin, N., Othman, S. H., Rashid, S. A., & Basha, R. K. (2020). Effects of glycerol and thymol on physical, mechanical, and thermal properties of corn starch films. *Food Hydrocolloids*, *106*, 105884.

Ollé Resa, C. P., Jagus, R. J., & Gerschenson, L. N. (2014). Effect of natamycin, nisin and glycerol on the physicochemical properties, roughness and hydrophobicity of tapioca starch edible films. *Materials Science and Engineering C*, *40*, 281–287.

Pierre, A. C., & Pajonk, M. (2002). *<aerogel_Pajonk_ChRev02_4243.pdf>*.

Takeshita, S., & Yoda, S. (2017). Translucent, hydrophobic, and mechanically tough aerogels constructed from trimethylsilylated chitosan nanofibers. *Nanoscale*, *9*(34), 12311–12315.

Ubeyitogullari, A., Brahma, S., Rose, D. J., & Ciftci, O. N. (2018). In Vitro Digestibility of Nanoporous Wheat Starch Aerogels. *Journal of Agricultural and Food Chemistry*, *66*(36), 9490–9497.

Ubeyitogullari, A., & Ciftci, O. N. (2016a). Formation of nanoporous aerogels from wheat starch. *Carbohydrate Polymers*, *147*, 125–132.

Ubeyitogullari, A., & Ciftci, O. N. (2016b). Formation of nanoporous aerogels from wheat starch. *Carbohydrate Polymers*, *147*, 125–132.

Wang, Yiwei, He, M., Wu, Y., Liu, Y., & Ouyang, J. (2021). Effect of Crosslinking Agents on the Physicochemical and Digestive Properties of Corn Starch Aerogel. *Starch/Staerke*, *73*(3–4), 1–34.

Wang, Yixin, Chen, X., Kuang, Y., Xiao, M., Su, Y., & Jiang, F. (2018). Microstructure and filtration performance of konjac glucomannan-based aerogels strengthened by wheat straw. *International Journal of Low-Carbon Technologies*, *13*(1), 67–75.

Wang, Y., Su, Y., Wang, W., Fang, Y., Riffat, S. B., & Jiang, F. (2019). The advances of polysaccharide-based aerogels: Preparation and potential application. *Carbohydrate polymers*, *226*, 115242.

White, R. J., Budarin, V. L., & Clark, J. H. (2008). Tuneable mesoporous materials from alpha-D-polysaccharides. *ChemSusChem*, *1*(5), 408–411.

Wu, B., Zhu, G., Dufresne, A., & Lin, N. (2019). Fluorescent Aerogels Based on Chemical Crosslinking between Nanocellulose and Carbon Dots for Optical Sensor. *ACS Applied Materials and Interfaces*, *11*(17), 16048–16058.

Xiao, J., Lv, W., Song, Y., & Zheng, Q. (2018). Graphene/nanofiber aerogels: Performance regulation towards multiple applications in dye adsorption and oil/water separation. *Chemical Engineering Journal*, *338*, 202–210.

Zamora-Sequeira, R., Ardao, I., Starbird, R., & García-González, C. A. (2018). Conductive nanostructured materials based on poly-(3,4-ethylenedioxythiophene) (PEDOT) and starch/κ-carrageenan for biomedical applications. *Carbohydrate Polymers*, *189*, 304–312.

Zeng, Z., Ma, X. Y. D., Zhang, Y., Wang, Z., Ng, B. F., Wan, M. P., & Lu, X. (2019). Robust Lignin-Based Aerogel Filters: High-Efficiency Capture of Ultrafine Airborne Particulates and the Mechanism. *ACS Sustainable Chemistry and Engineering*, *7*(7), 6959–6968.

Zheng, Q., Tian, Y., Ye, F., Zhou, Y., & Zhao, G. (2020). Fabrication and application of starch-based aerogel: Technical strategies. *Trends in Food Science & Technology*, *99*, 608-620.

Zhu, F. (2019). Starch based aerogels: Production, properties and applications. *Trends in Food Science & Technology*, *89*, 1-10.

Zhu, J., Hu, J., Jiang, C., Liu, S., & Li, Y. (2019). Ultralight, hydrophobic, monolithic konjac glucomannan-silica composite aerogel with thermal insulation and mechanical properties. *Carbohydrate Polymers*, *207*, 246–255.